

# Robust Single-Walled Carbon Nanotube-Coated Aramid Fibers with Tunable Conductivities for Broadband Radar Absorption in Honeycomb Structures

Huahui Tian,<sup>○</sup> Quanfen Guo,<sup>○</sup> Sicheng Liu,<sup>○</sup> Kun Jiao,<sup>○</sup> Xuanguang Ren, Jiayi Liu, He Hao, Jianbo Yin, Jin Long, Yi Wang, Jian Hu, Jinhui Yang, Yao Cheng,\* Xin Gao,\* and Jin Zhang\*

Cite This: <https://doi.org/10.1021/acsnano.5c05311>

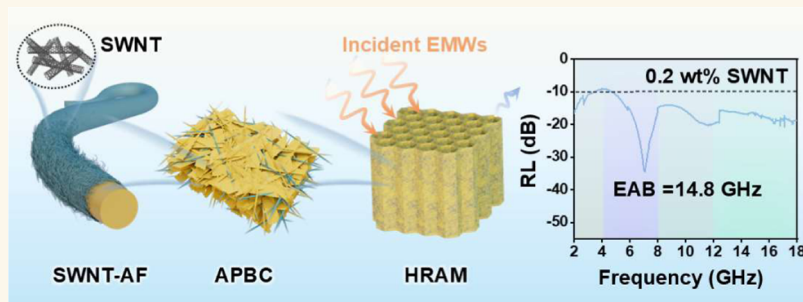
Read Online

ACCESS |

Metrics & More

Article Recommendations

Supporting Information



**ABSTRACT:** Single-walled carbon nanotubes (SWNTs), renowned for their high strength and electromagnetic properties, provide a potential solution for next-generation honeycomb-structured radar-absorbing materials (HRAMs). However, the integration of SWNTs into HRAMs is hindered by challenges including poor dispersion, wash-off loss, and the absence of scalable, compatible fabrication methods. Herein, we address these challenges by synthesizing tunable conductive SWNT-coated aramid fibers (SWNT-AF) via a continuous dip-coating method and integrating them into aramid paper-based composites (APBC) to fabricate HRAMs. The SWNT-AF serve as both structural reinforcements and dielectric loss centers within APBC, avoiding direct dispersion of SWNTs into the pulp and thereby mitigating agglomeration and wash-off loss. The optimized APBC, reinforced with these tailored fibers, exhibit improved dielectric properties, resulting in enhanced microwave absorption performance. The fabricated HRAMs achieve an effective absorption bandwidth of 14.8 GHz (2.0–18.0 GHz) with an ultralow SWNT loading of 0.2 wt % and a thin thickness of only 30 mm, demonstrating a reflection loss of  $-47.78$  dB. These results highlight the potential of SWNT-AF as lightweight, broadband radar-absorbing materials for stealth applications.

**KEYWORDS:** single-walled carbon nanotubes, aramid fibers, wet chemical dip-coating, honeycomb structure, broadband radar absorption

## INTRODUCTION

The rapid advancements in aerospace technologies have increased the demand for materials that are lightweight, structurally robust, and capable of efficiently absorbing broadband electromagnetic (EM) waves to reduce radar cross sections (RCS).<sup>1–9</sup> Among various candidates, honeycomb-structured radar-absorbing materials (HRAMs) have attracted significant attention because of their specific architecture. This architecture combines high strength with a multiscale wave dissipation mechanism, positioning HRAMs as a promising solution for next-generation radar-absorbing

applications.<sup>10–13</sup> However, conventional HRAMs, typically incorporating metallic matrices and magnetic fillers such as ferrites or conductive polymers,<sup>14–17</sup> exhibit several limitations, including poor environmental stability, high density, and

**Received:** March 28, 2025

**Revised:** May 19, 2025

**Accepted:** May 20, 2025

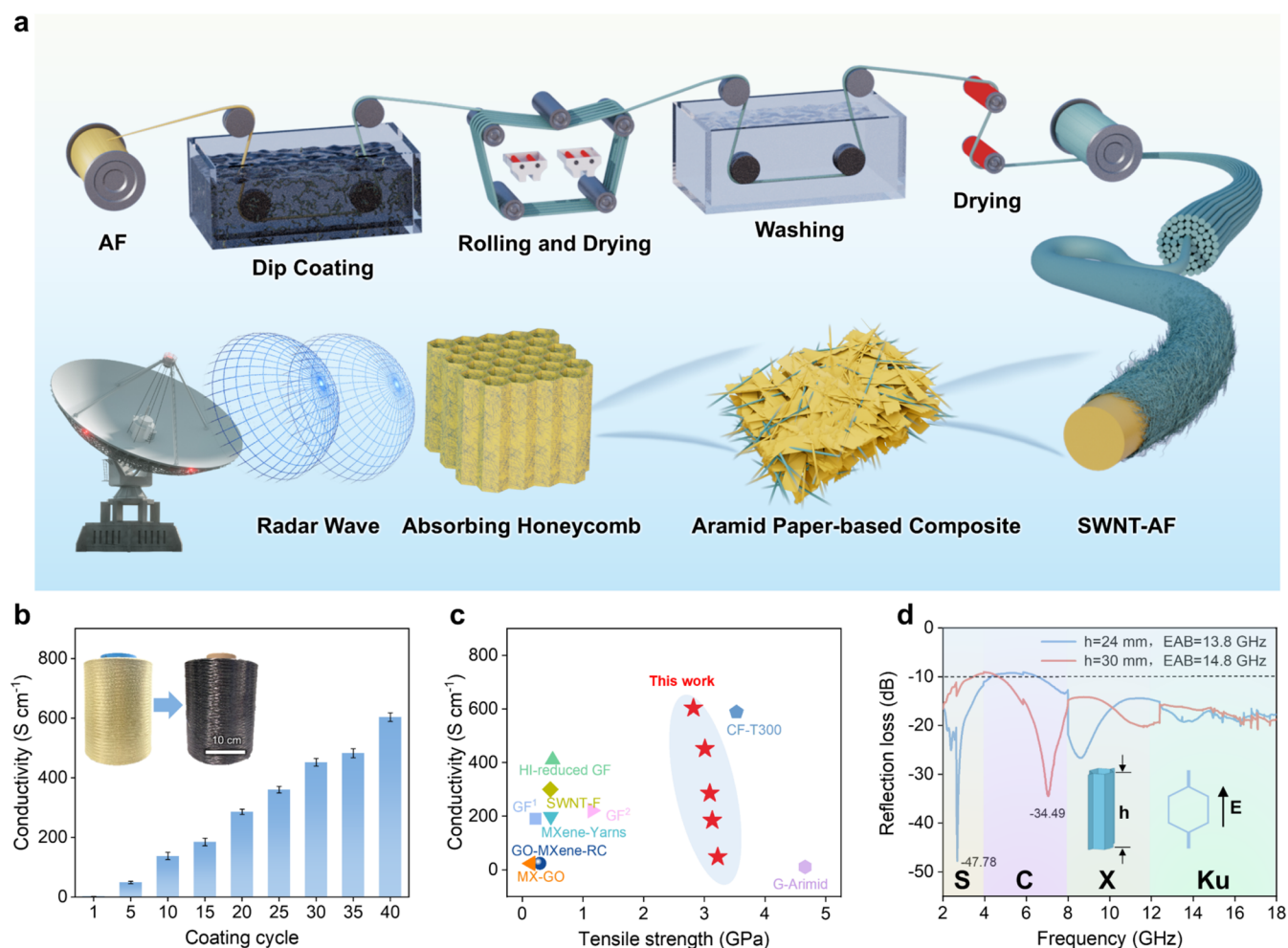


**Figure 1.** SWNT-coated aramid fibers (SWNT-AF) and their enhanced paper-based radar-absorbing honeycombs. (a) Schematic of the preparation of the SWNT-AF and their incorporation in radar-absorbing honeycombs, with SWNT-AF integrated into aramid paper-based composites (APBC). (b) Conductivity of SWNT-AF as a function of dip-coating cycle numbers, with inset digital photographs showing AF (yellow) and SWNT-AF (black). (c) Comparison of mechanical and electrical properties between SWNT-AF and other conductive fibers (detailed data in Table S1). (d) Absorption performance of paper-based radar-absorbing honeycombs with varying thickness (2.0–18.0 GHz) containing 3 wt % SWNT<sub>15</sub>-AF. SWNT<sub>15</sub>-AF denotes SWNT-coated aramid fibers prepared via 15 dip-coating cycles.

processing challenges. These limitations restrict their application in advanced aerospace systems requiring both lightweight design and long-term durability.

To overcome these limitations, aramid/carbon-based honeycomb-structured radar-absorbing materials (AC-HRAMs) have emerged as a promising alternative. AC-HRAMs employ aramid fibers (AF) and aramid fibrils (AFB) to form aramid paper as the honeycomb matrix, improving environmental stability while preserving the high-strength and lightweight attributes of HRAMs. Carbon-based absorbers,<sup>18–21</sup> including carbon nanotubes (CNTs) and carbon fibers (CFs), are incorporated into the matrix, imparting tunable electrical properties that facilitate efficient absorption of broadband EM waves and RCS reduction. This design not only improves environmental stability but also enhances mechanical robustness and offers flexibility in optimizing EM properties.

Two primary fabrication strategies are currently employed for AC-HRAMs: honeycomb-cell filling<sup>22–25</sup> and honeycomb-framework modification.<sup>15,26–29</sup> The honeycomb-cell filling method involves embedding carbon-based absorbers, such as nickel-coated multiwalled carbon nanotube/polyimide (Ni@CNT/PI) composites<sup>22</sup> and reduced graphene oxide (RGO)/

nonwoven absorbent composites,<sup>23</sup> into honeycomb cavities. Although effective, this approach demands high filler loadings, which may impair the lightweight attributes of AC-HRAMs. In contrast, the honeycomb-framework modification method either deposits carbon-based absorbers onto the honeycomb walls or incorporates them into the aramid paper matrix<sup>29</sup> to achieve efficient EM waves absorption. However, challenges including agglomeration and wash-off of carbon nanomaterial absorbers often result in inconsistent performance, while inefficient utilization of carbon nanomaterials restricts their practical applications.

Here, we propose incorporating structural-functional integrated, carbon-based conductive fibers directly into aramid paper as absorbers to fabricate HRAMs with superior performance. However, to date, few studies have explored this concept in HRAM systems. Some recent attempts are outlined below. Wang et al.<sup>29</sup> demonstrated the broadband microwave-absorbing capabilities of AC-HRAMs fabricated from paper-based composites (PBC) containing 3 wt % short carbon fibers, achieving excellent performance across 2.0–2.5 and 4.4–18 GHz. Furthermore, leveraging the compatibility of AF with aramid paper, Wu et al.<sup>30</sup> employed a layer-by-layer

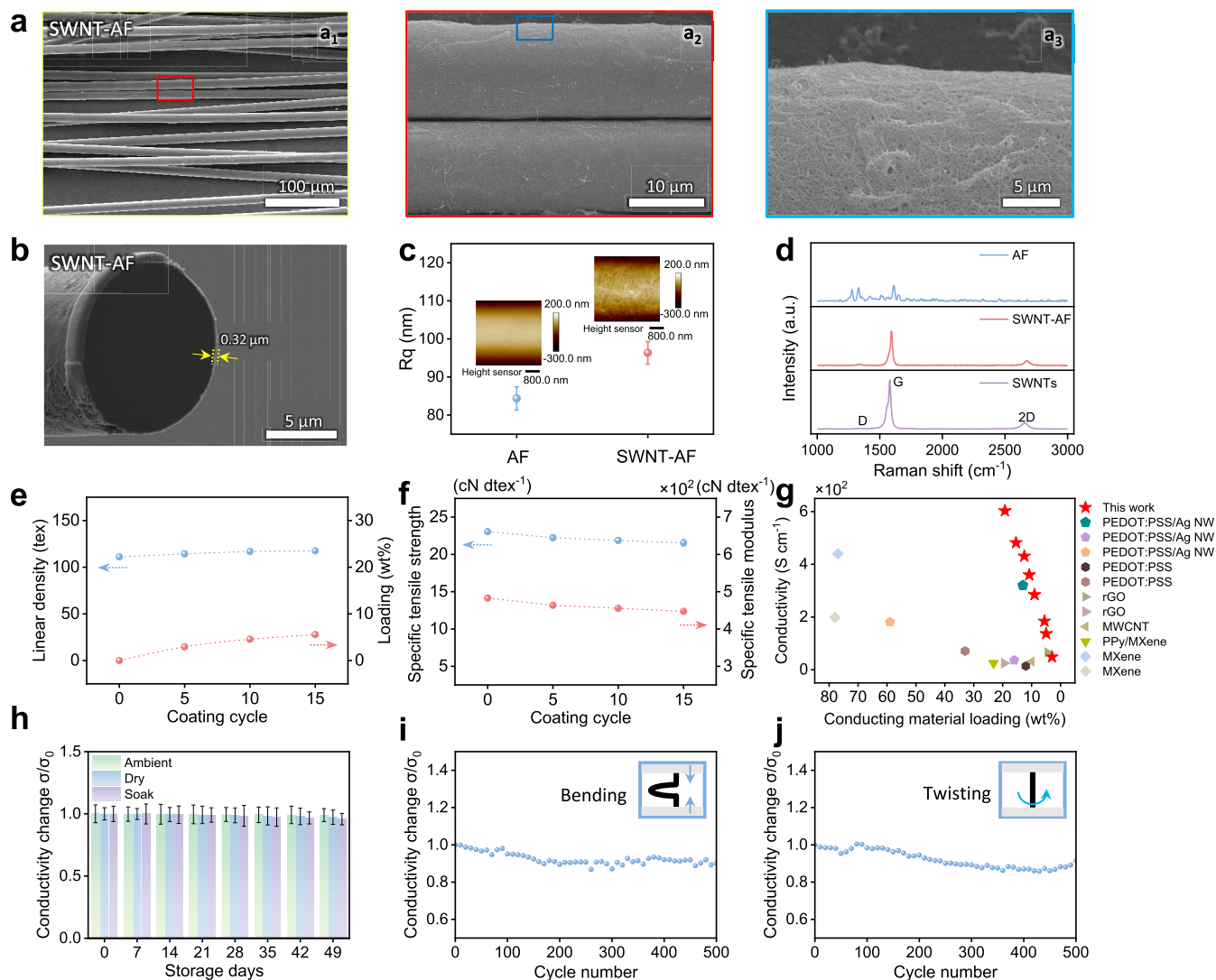


**Figure 2. Morphology, mechanical and electrical properties, and durability of SWNT-AF.** (a) Scanning electron microscopy (SEM) images of SWNT-AF. (b) Axial cross-sectional SEM image of SWNT-AF prepared via 15 dip-coating cycles. (c) Atomic force microscopy (AFM) images of AF and SWNT-AF, with root-mean-square (Rq) roughness values. (d) Raman spectra of AF, SWNT-AF, and SWNTs. (e) Linear density and SWNT loading of SWNT<sub>x</sub>-AF as a function of dip-coating cycles. (f) Mechanical performance of SWNT<sub>x</sub>-AF, including specific tensile strength and specific tensile modulus, with increasing dip-coating cycle numbers. (g) Comparison of conductivity and conductive filler loading between SWNT<sub>x</sub>-AF and reported conductive composite fibers (detailed data in Table S2). (h) Conductivity stability of SWNT<sub>15</sub>-AF over 7 weeks under different storage conditions: laboratory environment, desiccator (dry), and water immersion. (i, j) Conductivity retention of SWNT<sub>15</sub>-AF during (i) 500 bending cycles and (j) 500 twisting cycles.

self-assembly technique to coat AF and fibrils with CNTs, reducing CNT agglomeration and achieving a reflection loss below  $-10$  dB across the 8.0–12.0 GHz. Despite these efforts, AC-HRAMs still fail to achieve optimal performance due to the absence of an effective strategy for controllable CNT assembly on fibers and the inability to fine-tune the electrical properties of CNT-coated fibers in microwave-absorbing aramid paper. The electromagnetic properties of fiber-type absorbers can be tailored to target specific microwave wavelengths, thereby improving absorption performance.<sup>30–33</sup> Therefore, there is an urgent need for a strategy that not only prevents CNT agglomeration and detachment<sup>34–37</sup> but also optimizes the electrical properties of CNT-coated fibers, fully realizing the potential of AC-HRAMs for radar wave absorption.

In this work, we report a continuous dip-coating strategy to fabricate structural-functional integrated SWNT-coated aramid

fibers (SWNT<sub>x</sub>-AF, where  $x$  denotes the number of dip-coating cycles) (Figure 1a). The conductivity of SWNT<sub>x</sub>-AF can be systematically adjusted from 2.03 to 602.88 S cm<sup>-1</sup>, with mechanical properties minimally compromised (retaining  $\geq 84.9\%$  of their original strength), significantly outperforming previously reported composite fibers and commercial carbon fibers (Figure 1b, c). By coating SWNTs onto AF, SWNT<sub>x</sub>-AF serves as both structural reinforcements and dielectric loss centers within aramid paper-based composites (APBC). This design avoids direct dispersion of SWNTs into the pulp matrix, thereby preventing agglomeration and wash-off loss. The APBC honeycombs achieve an unprecedented effective absorption bandwidth (EAB) of 14.8 GHz (2.0–18.0 GHz) and a reflection loss of  $-47.78$  dB at an ultralow SWNT loading of 0.2 wt % and a thickness of 30 mm (Figure 1d), establishing new benchmarks for lightweight microwave-absorbing materials. This work not only addresses long-

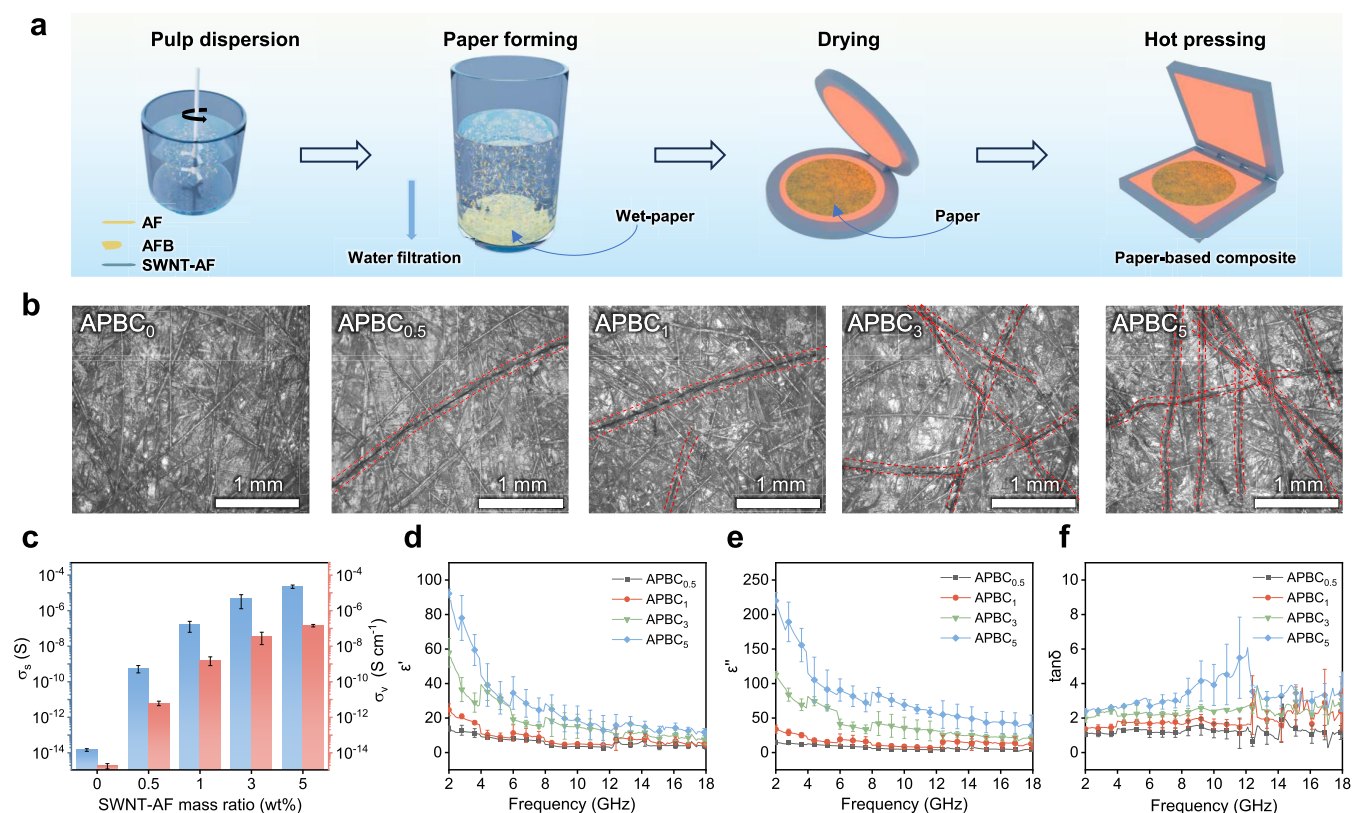


**Figure 3.** SWNT-AF enhanced aramid paper-based composites (APBC). (a) Schematic Illustration of the Preparation Process for APBC. (b) Optical micrographs of APBC with SWNT<sub>15</sub>-AF marked by red dashed lines. Composites labeled APBC<sub>0</sub>-APBC<sub>5</sub> correspond to 0–5 wt % SWNT-AF content. (c) Surface and volume electrical conductivity of APBC as a function of SWNT-AF content. (d–f) Dielectric properties of APBC: (d) real part  $\epsilon'$ , (e) imaginary part  $\epsilon''$ , and (f) loss tangent ( $\tan \delta$ ) of the dielectric constant.

standing challenges in AC-HRAM fabrication but also provides a scalable platform for integrating diverse nanomaterials, including MXenes and metallic nanowires, into multifunctional composites.

## RESULTS AND DISCUSSION

**Preparation and Characterization of SWNT-AF.** For the preparation of SWNT-coated fibers, we designed and fabricated a continuous automatic dip-coating device (Figure S1), which integrates continuous wet chemical dip-coating and roller drying processes. This device enables the conversion of insulating AF into core-sheath structured SWNT-coated aramid composite fibers, with conductivity adjustable by varying the number of coating cycles.

The aqueous dispersion of high-aspect-ratio SWNTs was prepared via ultrasound-assisted dispersion using sodium dodecyl sulfate (SDS) as a surfactant for the dip-coating method (Figures S2 and S3). The SDS molecules orient their hydrophobic alkyl tails toward the SWNT surface and hydrophilic head groups toward the aqueous phase, effectively reducing the interfacial energy between SWNTs and water and facilitating uniform dispersion of the SWNTs.<sup>38–41</sup> Significant aggregation of SWNTs was observed in the pure SWNT aqueous dispersion (Figure S4a), rendering it unsuitable for dip-coating AF. After the addition of SDS and ultrasonic treatment, the SWNTs exhibited a more uniform dispersion (Figure S4b,c); however, high SWNT concentrations still led to aggregation (Figure S4d). Therefore, a 2 mg mL<sup>-1</sup> SWNT aqueous dispersion was selected. The as-prepared SWNT dispersion remained stable for 7 weeks without precipitation

(Figure S5). Furthermore, kilometer-long AFs were continuously dip-coated using this dispersion at a drawing speed of 5 m min<sup>-1</sup> and collected at the end of each dip-coating cycle to evaluate the coating morphology, SWNT loadings, electrical properties, and mechanical characteristics.

The AF became conductive after the first dip-coating cycle, exhibiting a conductivity of  $2.03 \pm 0.21$  S cm<sup>-1</sup>. Scanning electron microscopy (SEM) images (Figure S6a) revealed that the SWNTs had not yet fully covered the AF surface, resulting in an incomplete conductive network. As the number of dip-coating cycles increased, the SWNT coverage improved, leading to enhanced conductivity (Figure S6b). The electrical conductivity of a 20-m-long SWNT-AF fiber was measured after 15 coating cycles, revealing a consistent conductivity of  $183.37 \pm 7.49$  S cm<sup>-1</sup> (Figure S7). The fiber transitioned from yellow to black (Figure 1b, inset), with the AF becoming uniformly wrapped by one-dimensional SWNTs, forming a mesh-like structure on the fiber surface. The shear force and pressure exerted by the rollers facilitated the stacking of SWNTs on the AF surface, resulting in a rough and dense SWNT network with a thickness of  $0.32 \mu\text{m}$  (Figures 2a–c and S8). The Raman spectra of AF before and after coating exhibited the characteristic D and G peaks of SWNTs (Figure 2d), further confirming the successful deposition of SWNTs on the AF surface. Notably, after 40 coating cycles, the SWNT-AF achieved a conductivity of  $602.88 \pm 2.11$  S cm<sup>-1</sup>, significantly outperforming most composite fibers and commercial carbon fibers (CF-T300).

The SWNT loading, linear density, and diameters of SWNT<sub>x</sub>-AF are presented in Figures 2e and S9. Even with a

lower SWNT loading, the resulting fibers exhibited electrical conductivity surpassing all previously reported values in the literature (Figure 2g). In terms of production efficiency, the automated dip-coating process demonstrated significant advantages over traditional manual methods. These results confirm that our method enables the controlled fabrication of conductive AF with tunable conductivity, offering a scalable and efficient approach for high-performance fiber production.

To further evaluate the stability of SWNT-AF, we assess the mechanical and electrical durability of as-prepared SWNT-AF. The mechanical properties of SWNT-AF showed only minor decreases after 15 cycles coating. Specifically, the specific tensile strength decreased slightly from 23.05 to 21.55 cN dtex<sup>-1</sup>, the specific tensile modulus decreased from 482.82 to 447.42 cN dtex<sup>-1</sup>, and the elongation at break slightly reduced from 4.12 to 3.98% (Figures 2f and S10). The retention rates of these mechanical properties were 93.5, 92.7, and 96.6%, respectively, meeting the requirements for various applications and rendering these fibers suitable for HRAMs fabrication.

The electrical stability of SWNT-AF was evaluated in three representative environments: a standard laboratory setting, a desiccator, and a water-soaked environment. Over a 7-week period, conductivity changes in these environments were recorded (Figure 2h). The results showed minimal conductivity loss, with decreases of only 0.96, 2.67, and 4.21% in the laboratory, dry, and water-soaked environments, respectively. In the laboratory environment, ambient humidity plays a critical role. Water molecules adsorb on SWNT interfaces, forming a lubricating hydration layer that mitigates stress and maintains electron transport networks. Moderate humidity enables self-limiting oxidation of SWNT edge defects, passivating reactive sites. Collectively, these effects result in a mere 0.96% conductivity loss.<sup>42,43</sup> In the desiccator's dry environment, lacking humidity-induced plasticization, interfacial stress induces microcracks in the SWNT network. This stress disrupts electron transport at nanotube junctions, increasing contact resistance. However, it only causes a 2.67% conductivity loss without macroscopic damage. In the water-soaked environment, long-term immersion detaches trace SWNTs. Multiple drying cycles subject the material to capillary-force-induced cyclic mechanical strain during water evaporation, exacerbating conductive network disconnections. Collectively, these factors lead to a 4.21% conductivity loss.<sup>44</sup> The mechanical stability of SWNT-AF was further evaluated under cyclic deformation conditions. After 500 cycles of 180° bending and 360° twisting, the conductivity retention rates were 90.06 and 91.47%, respectively (Figure 2i, j). These findings collectively demonstrate the excellent stability of SWNT-AF fibers, minimizing absorber loss due to potential SWNT wash-off during the APBC papermaking process.

**SWNT-AF Enhanced Aramid Paper Composites.** The tunable conductivity and high strength of SWNT-AF make them suitable for fabricating aramid paper (AP)-based composites (APBC) for microwave-absorbing applications. Typically, AP is composed of short AF and AFB. AF impart structural stiffness, while AFB improve interfacial adhesion between AF.<sup>45–48</sup> The geometric shape and arrangement of these fibers are critical factors in determining the physical properties of the paper matrix. Herein, we replace a small portion of AF with tailored SWNT-AF in APBC, enabling wide-range regulation of the electromagnetic parameters of APBC while maintaining other properties.

The APBC in this study were prepared via a wet papermaking process (Figure 3a), which closely mirrors the production process of AP, ensuring scalability for large-scale manufacturing. Prior to papermaking, the surface of SWNT-AF was modified to enhance hydrophilicity, ensuring improved dispersion in water. This modification was realized via hydrophilic sizing treatment of SWNT-AF using the custom-built automatic dip-coating apparatus described earlier, which reduced the water contact angle on the fiber surface from 156.0 to 30.3° (Figure S11). Both AF and SWNT-AF were then cut into 6 mm lengths (the aspect ratio is 468). During the papermaking process, the fiber-to-fibril weight ratio was maintained at 5:5 (w/w), and the basis weight of the resulting APBC was controlled to 40.0 ± 0.5 g m<sup>-2</sup>. The proportion of SWNT-AF in the composites was varied from 0 to 5 wt %, resulting in the following APBC formulations: APBC<sub>0</sub>, APBC<sub>0.5</sub>, APBC<sub>1</sub>, APBC<sub>3</sub>, and APBC<sub>5</sub>.

Optical images of APBC show that SWNT-AF (marked with red dashed lines) are randomly distributed within the composite matrix, with increasing density as the SWNT-AF weight ratio increases (Figure 3b). Notably, no SWNT agglomeration is observed, highlighting the effectiveness of our method in controlling SWNT within APBC. Figure 3c presents the surface electrical conductivity ( $\sigma_s$ ) and volume electrical conductivity ( $\sigma_v$ ) of APBC. Since AF and AFB are insulating materials, the surface and volume electrical conductivities of pure AF/AFB paper (APBC<sub>0</sub>) are 1.47 × 10<sup>-14</sup> S and 1.86 × 10<sup>-15</sup> S cm<sup>-1</sup>, respectively. The electrical conductivity of the composite paper increases significantly with increasing SWNT-AF mass fraction. However, the conductivity increase becomes less pronounced when the SWNT-AF content exceeds 1.0 wt %. Ultimately, APBC<sub>5</sub>, with the highest SWNT-AF content, achieves the highest electrical conductivity, with surface conductivity of 2.28 × 10<sup>-5</sup> S and volume conductivity of 1.45 × 10<sup>-7</sup> S cm<sup>-1</sup>. The introduction of conductive SWNT-AF significantly enhances the electrical conductivity of APBC, indicating the formation of a conductive network within the paper matrix. This network, combined with dipole polarization, interfacial polarization, and ohmic loss, facilitates the efficient conversion of microwave energy into thermal energy.<sup>49</sup>

Both SWNTs and aramid matrix are inherently nonmagnetic materials, exhibiting relative magnetic permeability  $\mu_r$  close to 1 (Figure S12). Consequently, microwave absorption performance of the composite is predominantly governed by dielectric loss mechanisms. The real part  $\epsilon'$  and imaginary part  $\epsilon''$  of the complex permittivity of APBC reflect the material's ability to store and dissipate electromagnetic energy. As the substrate material for HRAM, APBC must possess an optimized permittivity. An insufficiently low permittivity induces microwave transmission through the composite structure, whereas an excessively high permittivity promotes wave reflection, both of which critically degrade the radar-absorbing performance. Therefore, the complex permittivity of APBC in the 2.0–18.0 GHz frequency range was measured using a rectangular waveguide system, as shown in Figure 3d–f. Within this frequency range, both  $\epsilon'$  and  $\epsilon''$  decrease with increasing frequency, a fundamental requirement for broadband wave-absorbing materials. To elucidate the underlying dielectric loss mechanisms, we conducted a detailed analysis of the relaxation behavior using the Cole–Cole model.<sup>50</sup> The results (Figure S13) reveal distinct polarization and conduction mechanisms across different frequency regions. In the high-frequency region

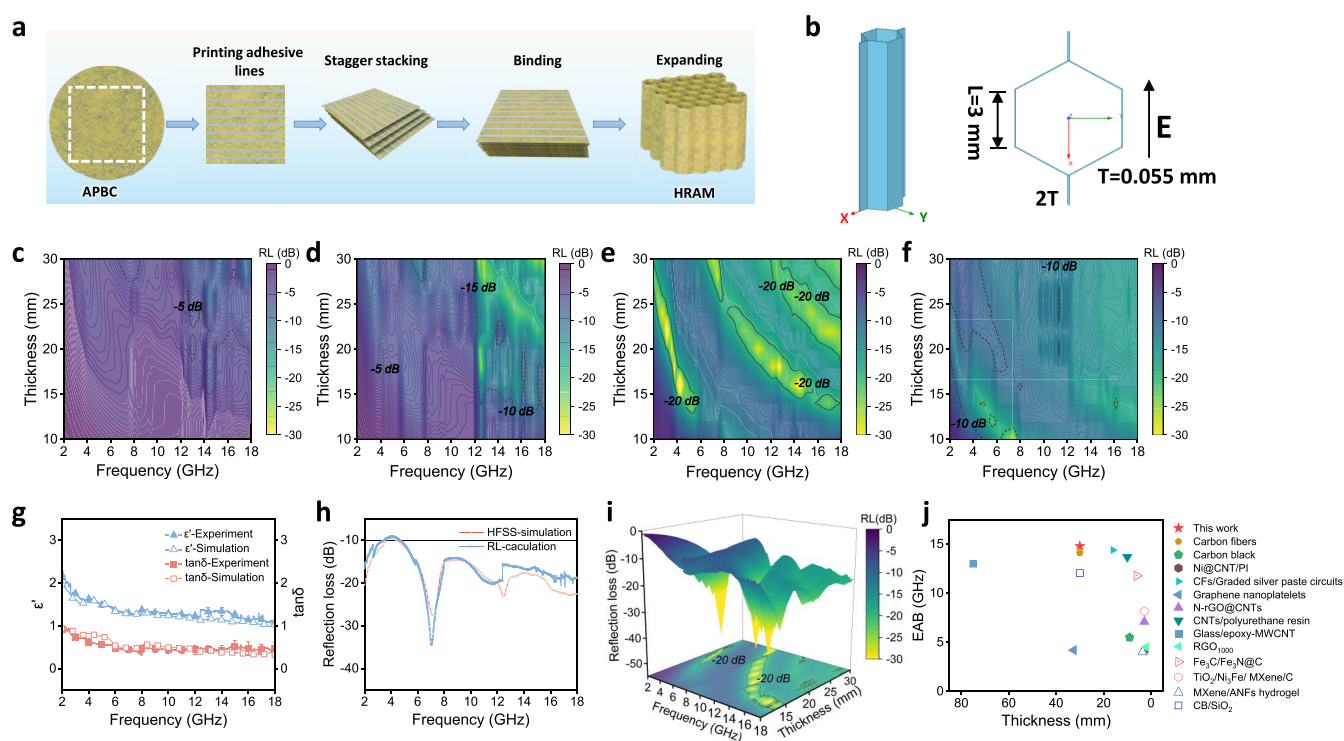


**Figure 4.** Microwave absorption properties of HRAM. (a) Schematic illustration of HRAM preparation process. (b) Single-cell honeycomb model (side length: 3 mm, wall thickness: 0.055 mm) and simulated reflection loss (RL) spectra for (c) HRAM<sub>0.5</sub>, (d) HRAM<sub>1</sub>, (e) HRAM<sub>3</sub>, and (f) HRAM<sub>5</sub> in the 2.0–18.0 GHz band as a function of honeycomb thickness. (g) Comparison of simulated vs experimental real permittivity ( $\epsilon'$ ) and loss tangent ( $\tan \delta$ ) for HRAM<sub>3</sub>. (h) Simulated vs experimental RL spectra for 30 mm-high HRAM<sub>3</sub>. (i) Experimentally measured RL of HRAM<sub>3</sub> at different thicknesses. (j) Comparison of EAB and the thickness for various microwave-absorbing composites (detailed data in Table S3). Our design achieves a record-high EAB of 14.8 GHz at a lower thickness of 30 mm and absorber loading (0.2 wt %), demonstrating the advantages of the structural-functional integration strategy based on SWNT-AF and honeycomb architecture.

(8.0–18.0 GHz), the Cole–Cole plots display multiple semicircles, indicative of overlapping relaxation processes arising from interfacial polarization and defect-induced dipole interactions. Specifically, Maxwell–Wagner polarization stems from charge accumulation at the interfaces between SWNTs and the aramid matrix, while dipolar relaxation is attributed to localized defects in the SWNT network. These synergistic mechanisms enhance dielectric loss at elevated frequencies. In contrast, the low-frequency region (2.0–8.0 GHz) exhibits a linear trend in the Cole–Cole plots, signifying a dominant contribution from conductive loss. As the SWNT-AF content increases from 0.5 to 5 wt %, the relaxation semicircles become less pronounced, while the linear segments become more distinct, indicating that improved network connectivity enhances charge transport and ohmic dissipation. At any fixed frequency,  $\epsilon'$ ,  $\epsilon''$ , and the dielectric loss tangent ( $\tan \delta$ ) all increase with rising SWNT-AF content. For instance, at 10 GHz, the complex permittivities of APBC<sub>0.5</sub>, APBC<sub>1</sub>, APBC<sub>3</sub>, and APBC<sub>5</sub> are (3.57–4.74j), (5.05–8.52j), (15.19–35.74j), and (19.11–69.03j), respectively, with corresponding  $\tan \delta$  values of 1.28, 1.66, 2.37, and 3.92. Given the relatively low SWNT loading (6.55 wt %) in SWNT-AF, increasing the proportion of SWNT-AF results in only a slight increase in SWNT content in the composite paper (e.g., 0.33 wt % in APBC<sub>5</sub>), thereby preserving the lightweight characteristics of the paper matrix. These results demonstrate that even at low SWNT loadings, APBC fabricated with SWNT-AF achieves efficient SWNT utilization, significantly improving the dielectric properties of the composite paper.

The microwave absorption properties of materials depend on impedance matching between the material and air, as well as the material's microwave attenuation capability. Within APBC, overlapping SWNT-AF in the composite paper form a millimeter-scale three-dimensional conductive network. In this network, electron hopping or migration within SWNTs dissipates microwave energy, leading to conductive losses and significantly enhancing microwave attenuation.<sup>51,52</sup> Furthermore, based on the absorber's structural configuration, APBC materials with optimized permittivity require careful selection to achieve impedance matching. This enables efficient microwave penetration into the absorber's interior, where progressive attenuation occurs through energy dissipation mechanisms.

**APBC Based Radar-Absorbing Honeycomb.** When APBC are fabricated into a honeycomb structure with regular hexagonal pores, the air within the pores facilitates the propagation of microwaves into the honeycomb interior, inducing multiple reflections and scattering. This extended propagation path enhances electromagnetic wave attenuation and facilitates efficient energy dissipation. However, it should be noted that excessive addition of SWNT-AF to the composite paper increases both conductivity and permittivity, potentially leading to impedance mismatch and significant microwave reflection. According to the quarter-wavelength matching theory (expressed as  $t_m = \frac{\lambda}{4} \sqrt{\mu_r \epsilon_r}$ , where  $t_m$  is the matching thickness,  $\lambda$  is the microwave wavelength, and  $\mu_r$  and  $\epsilon_r$  are the complex permeability and permittivity, respectively), the absorber thickness is intimately linked to the frequency at

which peak microwave absorption occurs.<sup>53,54</sup> When the material thickness satisfies the quarter-wavelength condition, destructive interference between waves reflected at the air-material interface and internal reflections leads to minimized reflection loss. Therefore, carefully tuning both the SWNT-AF content and honeycomb thickness is essential for optimizing the microwave absorption performance of APBC-based HRAMs. Here, we fabricated HRAM using SWNT-AF enhanced APBC to study and optimize their microwave absorption performance. The preparation process of the HRAM is schematically illustrated in Figure 4a. The hexagonal unit walls of the HRAM are composed exclusively of SWNT-AF enhanced APBC, with the interior filled with air. The microwave absorption properties of SWNT-AF enhanced HRAMs were evaluated via both theoretical and experimental approaches.

To simulate the absorption performance of the HRAM, a honeycomb unit cell model with a side length of 3.0 mm and a wall thickness of 0.055 mm was established (Figure 4b), with the electric field oriented parallel to the honeycomb's double wall. Using the complex effective permittivity of APBC, high-frequency structure simulator (HFSS) software was used to simulate the microwave reflection loss (RL) of APBC-based HRAMs with different SWNT<sub>15</sub>-AF contents over the 2.0–18.0 GHz frequency range as a function of thickness (Figure 4c–f). Simulation results show that HRAM<sub>0.5</sub> (containing 0.5 wt % SWNT<sub>15</sub>-AF) acts as a microwave-transmissive material (Figure 4c) due to the low permittivity and  $\tan\delta$  of APBC<sub>0.5</sub>. HRAM<sub>1</sub> (containing 1.0 wt % SWNT<sub>15</sub>-AF) exhibits effective microwave absorption (RL < -10 dB) in the 6.6–18.0 GHz band (Figure 4d), achieving an EAB of 7.4 GHz at a honeycomb thickness of 30 mm. HRAM<sub>3</sub> (containing 3.0 wt % SWNT<sub>15</sub>-AF) exhibits the widest EAB of 15.4 GHz at a honeycomb thickness of 30 mm, though it fails to effectively absorb microwaves in the 3.7–4.3 GHz band. Notably, at a honeycomb thickness of 18 mm and a frequency of 5.8 GHz, the minimum return loss ( $RL_{\min}$ ) reaches -49.30 dB (Figure 4e). HRAM<sub>5</sub> (containing 5.0 wt % SWNT<sub>15</sub>-AF) also demonstrates a broad EAB of 14.9 GHz at a honeycomb thickness of 18 mm (Figure 4f). Simulation results indicate that when the SWNT<sub>15</sub>-AF content does not exceed 3.0 wt %, the wave absorption capability of the HRAM improves with increasing SWNT<sub>15</sub>-AF content. Normalized impedance analysis reveals that HRAM<sub>3</sub> exhibits an impedance matching ratio ( $|Z_{in}/Z_0|$ ) approaching 1 near 7 GHz (Figure S14a), while the attenuation constant ( $\alpha$ ) increases with frequency (Figure S14b), indicating efficient microwave penetration and energy dissipation. This synergistic effect culminates in a pronounced absorption peak at 7 GHz. However, at a content of 5.0 wt %, the EAB of HRAM<sub>5</sub> is smaller than that of HRAM<sub>3</sub> due to impedance mismatch, indicating that higher SWNT<sub>15</sub>-AF content does not necessarily improve microwave absorption. Ultimately, HRAM<sub>3</sub> is selected as the optimal absorbing honeycomb structure.

Experimentally, an HRAM<sub>3</sub> (side length is 3.0 mm, thickness is 3.0 mm, containing 3.0 wt % SWNT<sub>15</sub>-AF) was fabricated, and its electromagnetic parameters were measured (Figures 4g, S15 and S16). The complex permittivity at 2.0 and 10.0 GHz were measured as (2.19–2.02j) and (1.29–0.57j), respectively, with dielectric loss  $\tan\delta$  of 0.92 and 0.44. Compared to APBC<sub>3</sub>, the real and imaginary parts of the effective permittivity of HRAM<sub>3</sub> were significantly lower, primarily due to the normalization of effective permittivity over the

entire HRAM volume, which contains large air voids. Additionally, the frequency-dependence trends of effective permittivity and dielectric loss tangent for HRAM<sub>3</sub> over the 2.0–18.0 GHz range mirrored those of APBC<sub>3</sub>, both decreasing with increasing frequency. The measured complex permittivity values of HRAM<sub>3</sub> closely matched the simulated results, confirming consistency between experimental and theoretical data. Both the simulated and experimentally measured RL spectra for 30 mm-high HRAM<sub>3</sub> exhibited similar results, with absorption peaks at 7.20 and 7.05 GHz, respectively (Figures 4h and S17).

Using the experimentally measured electromagnetic parameters of HRAM<sub>3</sub>, the microwave reflection loss (RL) across the 2.0–18.0 GHz range was calculated for thicknesses ranging from 10 to 40 mm (Figure 4i). This analysis demonstrates that SWNT-AF enhanced HRAMs can achieve broadband microwave absorption even with low SWNT absorbent loading. Specifically, HRAM<sub>3</sub> with a thickness of 24 mm achieved a minimum RL of -47.78 dB at 2.69 GHz (Figures 1d and 4i). The EAB reached its maximum of 14.8 GHz at a thickness of 30 mm (Figure S18), with a corresponding minimum RL of -34.49 dB at 7.05 GHz. Interestingly, as the thickness of HRAM<sub>3</sub> increased, its microwave absorption capability at 2.0 GHz first increased and then declined. The most prominent absorption occurred at 26 mm, where a reflection loss of -20.30 dB was observed (Figure S19), indicating that HRAM<sub>3</sub> is a promising candidate for low-frequency microwave absorption. Compared with recently reported state-of-the-art microwave-absorbing materials (Figures 4j, S20, Table S3), Our design achieves a record-high EAB of 14.8 GHz at a lower thickness of 30 mm and absorber loading of 0.2 wt %, demonstrating the advantages of the structural-functional integration strategy based on SWNT-AF and honeycomb architecture.

## CONCLUSIONS

This study presents a continuous wet chemical dip-coating method that effectively functionalizes fiber surfaces with carbon nanocomposites, promoting the large-scale application of carbon nanomaterials in wave-absorbing composite materials. By leveraging a customized automatic dip-coating system, SWNTs were uniformly coated onto the surface of AF, enabling the controlled preparation of aramid composite fibers (SWNT-AF) with adjustable conductivity ranging from 2.03 to 602.88 S cm<sup>-1</sup>. The SWNT coating exhibited robust structural stability, meeting the mechanical demands of wet papermaking processes. Incorporating SWNT-AF into APBC avoided SWNT agglomeration and wash-off losses inherent in direct SWNT addition to pulp. The SWNT content in the composite paper was precisely controlled between 0.03 and 0.33 wt %, resulting in significantly enhanced dielectric constant and loss tangent values. The resulting HRAMs achieved a record-EAB of 14.8 GHz (92.50% coverage of the 2.0–18.0 GHz band) at a thickness of 30 mm, with a minimum RL of -49.30 dB. This work establishes a versatile platform for advanced HRAMs, applicable to diverse microwave-absorbing nanomaterials (e.g., graphene, MXenes, metal nanowires), and paves the way for next-generation lightweight, high-strength, and broadband radar-absorbing composites.

## EXPERIMENTAL SECTION

**Materials and Reagents.** Single-walled carbon nanotubes (SWNTs, diameter: 1–2 nm, length: 5–30  $\mu$ m, purity >95%) were

purchased from Jiangsu Xianfeng Nanomaterials Technology Co., Ltd., poly(p-phenylene terephthalamide) (PPTA) was provided by Bluestar Chengrand Co., Ltd., sodium dodecyl sulfate (SDS,  $\geq 95\%$ ) was purchased from Sigma-Aldrich, short AF, and AFB were procured from suppliers.

**Preparation of 2 mg mL<sup>-1</sup> SWNT Dispersion.** First, 1.0 g of sodium dodecyl sulfate (SDS) was dissolved in 200 mL of deionized water under magnetic stirring until fully dissolved. Next, 0.4 g of SWNTs were added to the solution, followed by ultrasonication using a JY99-IIDN ultrasonic cell disruptor (1080 W) in an ice–water bath. The treatment was performed for 1 h with 20 min on/20 min off cycles, repeated three times, yielding a homogeneous SWNT dispersion. Finally, the dispersion was stored in a sealed container at room temperature.

**Preparation of APBC.** The composite paper was fabricated via a wet papermaking process involving pulping, sheet forming, drying, and hot pressing. Short SWNT<sub>15</sub>-AF, short aramid fibers (AF), and aramid fibrils (AFB) were separately dispersed in water using a KRK 2530 standard disintegrator at 3000 rpm for 60, 60, and 600 s, respectively. Following dispersion, the pulp was mixed and filtered using a PTI RK3AKWT paper machine to form aramid wet sheets. The wet sheets were then dried in a convection oven at 105 °C for 10 min. Finally, the dried sheets were hot-pressed at 290 °C and 10 MPa for 5 min to obtain APBC. By adjusting the ratio of short SWNT<sub>15</sub>-AF to short AF, microwave-absorbing paper with tunable carbon nanotube loadings was fabricated.

**Preparation of AC-HRAM.** First, double-sided tape with a width of 3 mm was applied to the upper surface of the composite paper, with a 9 mm spacing between adjacent strips. Then, the composite paper was glued layer by layer, ensuring that the tape on odd-numbered sheets was aligned with the midpoint between two adjacent tapes on even-numbered sheets. Next, the stacked aramid paper was cut and reassembled according to the desired thickness of the honeycomb structure, which was set at 3 mm in this study. To form the honeycomb structure, the laminated boards were stretched by attaching tape to the top and bottom layers of the composite paper and applying tension. This stretching action caused the nonadhesive parts of the composite paper to open, forming hexagonal honeycomb cells. Finally, heat treatment was applied to fix the structure. The side length of the honeycomb cells was 3 mm, and the thicknesses of the nonadhesive (single layer) and adhesive (double layer) parts were 0.055 and 0.125 mm, respectively.

## ASSOCIATED CONTENT

### Supporting Information

The Supporting Information is available free of charge at <https://pubs.acs.org/doi/10.1021/acsnano.5c05311>.

SEM images, TEM images, Raman spectra, and other graphs and data (PDF)

## AUTHOR INFORMATION

### Corresponding Authors

**Yao Cheng** – Beijing Graphene Institute (BGI), Beijing 100095, P. R. China; Email: [chengy@bgi-graphene.com](mailto:chengy@bgi-graphene.com)

**Xin Gao** – School of Materials Science and Engineering, Peking University, Beijing 100871, P. R. China; Beijing Graphene Institute (BGI), Beijing 100095, P. R. China; Academy for Advanced Interdisciplinary Studies, Peking University, Beijing 100871, P. R. China; Email: [gaoxin-cnc@pku.edu.cn](mailto:gaoxin-cnc@pku.edu.cn)

**Jin Zhang** – School of Materials Science and Engineering, Peking University, Beijing 100871, P. R. China; Beijing Graphene Institute (BGI), Beijing 100095, P. R. China; Beijing Science and Engineering Center for Nanocarbons, Beijing National Laboratory for Molecular Sciences, College of Chemistry and Molecular Engineering, Peking University,

Beijing 100871, P. R. China; [orcid.org/0000-0003-3731-8859](https://orcid.org/0000-0003-3731-8859); Email: [jinzhang@pku.edu.cn](mailto:jinzhang@pku.edu.cn)

## Authors

**Huahui Tian** – School of Materials Science and Engineering, Peking University, Beijing 100871, P. R. China; Beijing Graphene Institute (BGI), Beijing 100095, P. R. China; State Key Laboratory of High-efficiency Utilization of Coal and Green Chemical Engineering, College of Chemistry and Chemical Engineering, Ningxia University, Yinchuan 750021, P. R. China

**Quanfen Guo** – School of Materials Science and Engineering, Peking University, Beijing 100871, P. R. China; Beijing Graphene Institute (BGI), Beijing 100095, P. R. China

**Sicheng Liu** – School of Materials Science and Engineering, Peking University, Beijing 100871, P. R. China; School of Light Industry and Engineering, South China University of Technology, Guangzhou 510640, P. R. China

**Kun Jiao** – School of Materials Science and Engineering, Peking University, Beijing 100871, P. R. China; Beijing Graphene Institute (BGI), Beijing 100095, P. R. China

**Xuangang Ren** – Beijing Graphene Institute (BGI), Beijing 100095, P. R. China; Beijing Science and Engineering Center for Nanocarbons, Beijing National Laboratory for Molecular Sciences, College of Chemistry and Molecular Engineering, Peking University, Beijing 100871, P. R. China

**Jiayi Liu** – Beijing Graphene Institute (BGI), Beijing 100095, P. R. China; Academy for Advanced Interdisciplinary Studies, Peking University, Beijing 100871, P. R. China

**He Hao** – Beijing Science and Engineering Center for Nanocarbons, Beijing National Laboratory for Molecular Sciences, College of Chemistry and Molecular Engineering, Peking University, Beijing 100871, P. R. China

**Jianbo Yin** – Beijing Graphene Institute (BGI), Beijing 100095, P. R. China; State Key Laboratory of Photonics and Communications, School of Electronics and Academy for Advanced Interdisciplinary Studies, Peking University, Beijing 100871, P. R. China

**Jin Long** – School of Light Industry and Engineering, South China University of Technology, Guangzhou 510640, P. R. China; [orcid.org/0000-0002-9601-724X](https://orcid.org/0000-0002-9601-724X)

**Yi Wang** – School of Light Industry and Engineering, South China University of Technology, Guangzhou 510640, P. R. China

**Jian Hu** – School of Light Industry and Engineering, South China University of Technology, Guangzhou 510640, P. R. China

**Jinhui Yang** – State Key Laboratory of High-efficiency Utilization of Coal and Green Chemical Engineering, College of Chemistry and Chemical Engineering, Ningxia University, Yinchuan 750021, P. R. China; [orcid.org/0000-0002-9381-1560](https://orcid.org/0000-0002-9381-1560)

Complete contact information is available at: <https://pubs.acs.org/doi/10.1021/acsnano.5c05311>

## Author Contributions

<sup>○</sup>H.T., Q.G., S.L. and K.J. contributed equally to this work.

## Notes

The authors declare no competing financial interest.

## ACKNOWLEDGMENTS

This work was financially supported by the National Natural Science Foundation of China (Grant Nos. T2188101, 52021006, 52302034); the Ministry of Science and Technology of China (2022YFA1203302, 2022YFA1203304 and 2018YFA0703502); the Strategic Priority Research Program of CAS (XDB36030100); the Beijing National Laboratory for Molecular Sciences (BNLMS-CXTD-202001); and the Shenzhen Science and Technology Innovation Commission (KQTD20221101115627004). X.G. thanks the Fundamental Research Funds for the Central Universities, Peking University.

## REFERENCES

- (1) Zhao, Z.; Qing, Y.; Kong, L.; Xu, H.; Fan, X.; Yun, J.; Zhang, L.; Wu, H. Advancements in Microwave Absorption Motivated by Interdisciplinary Research. *Adv. Mater.* **2024**, *36*, No. 2304182.
- (2) Wu, Z.; Cheng, H. W.; Jin, C.; Yang, B.; Xu, C.; Pei, K.; Zhang, H.; Yang, Z.; Che, R. Dimensional Design and Core–Shell Engineering of Nanomaterials for Electromagnetic Wave Absorption. *Adv. Mater.* **2022**, *34*, No. 2107538.
- (3) Akram, M. R.; Ding, G.; Chen, K.; Feng, Y.; Zhu, W. Ultrathin Single Layer Metasurfaces with Ultra-Wideband Operation for Both Transmission and Reflection. *Adv. Mater.* **2020**, *32*, No. 1907308.
- (4) Gai, L.; Wang, Y.; Wan, P.; Yu, S.; Chen, Y.; Han, X.; Xu, P.; Du, Y. Compositional and Hollow Engineering of Silicon Carbide/Carbon Microspheres as High-Performance Microwave Absorbing Materials with Good Environmental Tolerance. *Nano-Micro Lett.* **2024**, *16*, No. 167.
- (5) Pan, F.; Shi, Y.; Yang, Y.; Guo, H.; Li, L.; Jiang, H.; Wang, X.; Zeng, Z.; Lu, W. Porifera-Inspired Lightweight, Thin, Wrinkle-Resistance, and Multifunctional MXene Foam. *Adv. Mater.* **2024**, *36*, No. 2311135.
- (6) Hao, Y.; Leng, Z.; Yu, C.; Xie, P.; Meng, S.; Zhou, L.; Li, Y.; Liang, G.; Li, X.; Liu, C. Ultra-Lightweight Hollow Bowl-Like Carbon as Microwave Absorber Owning Broad Band and Low Filler Loading. *Carbon* **2023**, *212*, No. 118156.
- (7) Han, G.; Wang, Q.; Ding, F.; Fang, M.; Fang, X.; Yi, P.; Li, Y.; Sun, X.; He, J.; Li, J.; Yu, R.; Shui, J.; Liu, X. Assembly of Partially Unzipped Multiwalled Carbon Nanotubes Into Ultralight, Highly Efficient and Multifunctional Electromagnetic Wave Absorbing Aerogel. *Carbon* **2023**, *213*, No. 118220.
- (8) Dai, B.; Ma, Y.; Dong, F.; Yu, J.; Ma, M.; Thabet, H. K.; El-Bahy, S. M.; Ibrahim, M. M.; Huang, M.; Seok, I.; Roymahapatra, G.; Naik, N.; Xu, B. B.; Ding, J.; Li, T. Overview of MXene and Conducting Polymer Matrix Composites for Electromagnetic Wave Absorption. *Adv. Compos. Hybrid Mater.* **2022**, *5*, 704–754.
- (9) Wang, X.; Xing, X.; Zhu, H.; Li, J.; Liu, T. State of the Art and Prospects of Fe<sub>3</sub>O<sub>4</sub>/Carbon Microwave Absorbing Composites From the Dimension and Structure Perspective. *Adv. Colloid Interface Sci.* **2023**, *318*, No. 102960.
- (10) Li, W.; Xu, L.; Zhang, X.; Gong, Y.; Ying, Y.; Yu, J.; Zheng, J.; Qiao, L.; Che, S. Investigating the Effect of Honeycomb Structure Composite On Microwave Absorption Properties. *Compos. Commun.* **2020**, *19*, 182–188.
- (11) Choi, W.-H.; Kim, C. Broadband Microwave-Absorbing Honeycomb Structure with Novel Design Concept. *Composites, Part B* **2015**, *83*, 14–20.
- (12) Lu, J.; Di, X.; Yuan, M.; Sun, B.; Zhou, C.; Luo, Y.; Chen, Y.; Zou, H. In-Situ Construction of Phase-Separated Interconnected PVA@RGO Frameworks Using Dual-Crosslinking/Reduction Steps for Broadband Microwave Absorption and Enhanced Structural Performance of Aramid Honeycombs. *Carbon* **2024**, *228*, No. 119360.
- (13) Liu, Z.; Zhang, R.; Wang, S.; Zhao, W.; Yu, G.; Wu, L. Design and Fabrication of an All-Composite Ultra-Broadband Absorbing Structure with Superior Load-Bearing Capacity. *Compos. Sci. Technol.* **2023**, *240*, No. 110094.
- (14) Ren, Z.; Liu, X.; Su, J.; Liu, Y.; Zou, H.; Tian, J.; Sun, X.; Du, X.; Yin, H. Low-Profile Broadband Microwave Absorber Based On Magnetic Coating and Artificial Electromagnetic Structures. *Chem. Eng. J.* **2023**, *466*, No. 143115.
- (15) Pang, H.; Duan, Y.; Dai, X.; Huang, L.; Yang, X.; Zhang, T.; Liu, X. The Electromagnetic Response of Composition-Regulated Honeycomb Structural Materials Used for Broadband Microwave Absorption. *J. Mater. Sci. Technol.* **2021**, *88*, 203–214.
- (16) Zhang, M.; Ling, H.; Ding, S.; Xie, Y.; Cheng, T.; Zhao, L.; Wang, T.; Bian, H.; Lin, H.; Li, Z.; Meng, A. Synthesis of CF@PANI Hybrid Nanocomposites Decorated with Fe<sub>3</sub>O<sub>4</sub> Nanoparticles Towards Excellent Lightweight Microwave Absorber. *Carbon* **2021**, *174*, 248–259.
- (17) Nam, Y.-W.; Choi, J.; Lee, W.; Kim, C. Thin and Lightweight Radar-Absorbing Structure Containing Glass Fabric Coated with Silver by Sputtering. *Compos. Struct.* **2017**, *160*, 1171–1177.
- (18) Kim, S. H.; Lee, S. Y.; Zhang, Y.; Park, S. J.; Gu, J. Carbon-Based Radar Absorbing Materials Toward Stealth Technologies. *Adv. Sci.* **2023**, *10*, No. 2303104.
- (19) Wen, L.; Yan, Z.; Zhu, Y.; Guan, L.; Guo, X.; Zhao, B.; Zhang, J.; Hao, J.; Zhang, R. Recent Progress On the Electromagnetic Wave Absorption of One-Dimensional Carbon-Based Nanomaterials. *J. Mater. Res. Technol.* **2023**, *26*, 2191–2218.
- (20) Li, H.; Yang, C.; Cheng, M.; Li, Z.; Bandaru, S.; Chen, W.; Shi, Y.; Zhang, J.; Liu, X.; Zhang, X. Multiscale Design of Carbon-Based, High-Efficiency and Wide-Frequency Microwave-Absorption Composites. *Ceram. Int.* **2021**, *47*, 20467–20475.
- (21) Jiang, B.; Qi, C.; Yang, H.; Wu, X.; Yang, W.; Zhang, C.; Li, S.; Wang, L.; Li, Y. Recent Advances of Carbon-Based Electromagnetic Wave Absorption Materials Facing the Actual Situations. *Carbon* **2023**, *208*, 390–409.
- (22) Wang, C.; Ma, S.; Li, D.; Zhao, J.; Zhou, H.; Wang, D.; Liu, C.; Wang, S.; Chen, C. Direct Ink Writing of Thermoresistant, Lightweight Composite Polyimide Honeycombs with Tunable X-Band Electromagnetic Wave Absorption Properties. *Addit. Manuf.* **2023**, *70*, No. 103554.
- (23) Li, H.; Bi, S.; Cai, J.; Chu, X.; Hou, G.; Zhang, J.; Wu, T. Reduced Graphene Oxide/Nonwoven Fabric Filled Honeycomb Composite Structure for Broadband Microwave Absorption. *Carbon* **2024**, *223*, No. 119005.
- (24) Lu, J.; Yuan, M.; Di, X.; Yuan, Q.; Ni, L.; Luo, Y.; Chen, Y.; Zou, H. Fast, Non-Carbonized, Ambient-Drying PVA/CNF@GO Foam: Towards Super-Broadband Microwave Absorption and Structural Strength Enhancement in Aramid Honeycomb. *Chem. Eng. J.* **2024**, *489*, No. 151385.
- (25) Xie, S.; Ji, Z.; Yang, Y.; Hou, G.; Wang, J. Electromagnetic Wave Absorption Properties of Honeycomb Structured Plasterboards in S and C Bands. *J. Build. Eng.* **2016**, *7*, 217–223.
- (26) Bi, S.; Zhao, Y.; Hou, G.; Zhang, J.; Li, H.; Song, Y.; Hou, Z.; Liu, Z. Microwave Absorption and Mechanical Properties of CNTs/PU Composites with Honeycomb Structure. *Appl. Compos. Mater.* **2022**, *29*, 1393–1407.
- (27) Pei, R.; Nan, K.; Wang, W.; Rao, H.; Li, Y.; Wang, Y. Rational Design of Hollow Bimetallic Sulfide@Carbon with Abundant Heterogeneous Interfaces and Conductive Network Synergies for Efficient Microwave Absorption. *Carbon* **2024**, *224*, No. 119099.
- (28) Zhou, Q.; Qi, C.; Shi, T.; Li, Y.; Ren, W.; Gu, S.; Xue, B.; Ye, F.; Fan, X.; Du, L. 3D Printed Carbon Based All-Dielectric Honeycomb Metastructure for Thin and Broadband Electromagnetic Absorption. *Composites, Part A* **2023**, *169*, No. 107541.
- (29) Wang, H.; Xiu, X.; Wang, Y.; Xue, Q.; Ju, W.; Che, W.; Liao, S.; Jiang, H.; Tang, M.; Long, J.; Hu, J. Paper-Based Composites as a Dual-Functional Material for Ultralight Broadband Radar Absorbing Honeycombs. *Composites, Part B* **2020**, *202*, No. 108378.
- (30) Wu, Y.; Chen, L.; Han, Y.; Liu, P.; Xu, H.; Yu, G.; Wang, Y.; Wen, T.; Ju, W.; Gu, J. Hierarchical Construction of CNT Networks in Aramid Papers for High-Efficiency Microwave Absorption. *Nano Res.* **2023**, *16*, 7801–7809.

- (31) Chu, Z.; Cheng, H.; Xie, W.; Sun, L. Effects of Diameter and Hollow Structure On the Microwave Absorption Properties of Short Carbon Fibers. *Ceram. Int.* **2012**, *38*, 4867–4873.
- (32) Wang, H.; Long, J.; Wang, Y.; Liang, Y.; Hu, J.; Jiang, H. The Influence of Carbon Fiber Diameter and Content On the Dielectric Properties of Wet-Laid Nonwoven Fabric. *Text. Res. J.* **2019**, *89*, 2542–2552.
- (33) Cao, M.-S.; Song, W.; Hou, Z.; Wen, B.; Yuan, J. The Effects of Temperature and Frequency On the Dielectric Properties, Electromagnetic Interference Shielding and Microwave-Absorption of Short Carbon Fiber/Silica Composites. *Carbon* **2010**, *48*, 788–796.
- (34) Zhang, S.; Li, W.; Wu, H.; Jiao, J. Multi-Optimized Flexible Graphene Oxide/Multi-Walled Carbon Nanotubes/Ferroferric Oxide Nanopaper with Enhanced Electromagnetic Wave Absorption Performance. *Adv. Compos. Hybrid Mater.* **2023**, *6*, 154.
- (35) Guo, S.; Cai, Y.; Cheng, L.; Huang, S.; Liu, T.; Yu, H.; Chen, D.; Wang, Y.; Hu, Z.; Zhou, Y. Fiber, Monolithic Fiber and Twisted Fiber Structures: Efficient Microwave Absorption via Surface-Modified Carbon Nanotube Buckypaper/Silicon Carbide-Based Self-Sealing Layered Composites. *J. Mater. Chem. A* **2024**, *12*, 5377–5391.
- (36) Chen, S. H.; Kuo, W. S.; Yang, R. B. Microwave Absorbing Properties of a Radar Absorbing Structure Composed of Carbon Nanotube Papers/Glass Fabric Composites. *Int. J. Appl. Ceram. Technol.* **2019**, *16*, 2065–2072.
- (37) Yin, Q.; Jia, H.; Liu, G.; Ji, Q. Tailoring the Mechanical Performance of Carbon Nanotubes Buckypaper by Aramid Nanofibers Towards Robust and Compact Supercapacitor Electrode. *Adv. Funct. Mater.* **2022**, *32*, No. 2111177.
- (38) Duan, W. H.; Wang, Q.; Collins, F. Dispersion of Carbon Nanotubes with SDS Surfactants: A Study From a Binding Energy Perspective. *Chem. Sci.* **2011**, *2*, 1407.
- (39) Chiodarelli, N.; De Volder, M. High-Throughput and Consistent Production of Aqueous Suspensions of Single-Wall Carbon Nanotubes. *Carbon* **2019**, *145*, 757–763.
- (40) Li, S.; Yan, J.; Zhang, Y.; Qin, Y.; Zhang, Y.; Du, S. Comparative Investigation of Carbon Nanotubes Dispersion Using Surfactants: A Molecular Dynamics Simulation and Experimental Study. *J. Mol. Liq.* **2023**, *377*, No. 121569.
- (41) Das, S. K.; Sengupta, S.; Velarde, L. Interfacial Surfactant Ordering in Thin Films of SDS-Encapsulated Single-Walled Carbon Nanotubes. *J. Phys. Chem. Lett.* **2016**, *7*, 320–326.
- (42) Jaber-Ansari, L.; Hahm, M. G.; Somu, S.; Sanz, Y. E.; Busnaina, A.; Jung, Y. J. Mechanism of Very Large Scale Assembly of SWNTs in Template Guided Fluidic Assembly Process. *J. Am. Chem. Soc.* **2009**, *131*, 804–808.
- (43) Cui, J.; Zhang, J.; Wang, X.; Theogene, B.; Wang, W.; Tohmyoh, H.; He, X.; Mei, X. Atomic-Scale Simulation of the Contact Behavior and Mechanism of the SWNT–AgNW Heterostructure. *J. Phys. Chem. C* **2019**, *123*, 19693–19703.
- (44) Bi, L.; Perry, W.; Wang, R. J.; Lord, R.; Hryhorchuk, T.; Inman, A.; Gogotsi, O.; Balitskiy, V.; Zahorodna, V.; Baginskiy, I.; Vorotilo, S.; Gogotsi, Y. MXene Functionalized Kevlar Yarn Via Automated, Continuous Dip Coating. *Adv. Funct. Mater.* **2024**, *34*, No. 2312434.
- (45) Du, Y.; Yan, N.; Kortschot, M. T. Light-Weight Honeycomb Core Sandwich Panels Containing Biofiber-Reinforced Thermoset Polymer Composite Skins: Fabrication and Evaluation. *Composites, Part B* **2012**, *43*, 2875–2882.
- (46) Uddin, M. N.; Gandy, H. T. N.; Rahman, M. M.; Asmatulu, R. Adhesiveless Honeycomb Sandwich Structures of Prepreg Carbon Fiber Composites for Primary Structural Applications. *Adv. Compos. Hybrid Mater.* **2019**, *2*, 339–350.
- (47) Shan, J.; Xu, S.; Zhou, L.; Wang, D.; Liu, Y.; Zhang, M.; Wang, P. Dynamic Fracture of Aramid Paper Honeycomb Subjected to Impact Loading. *Compos. Struct.* **2019**, *223*, No. 110962.
- (48) Yang, W.; Zhang, X.; Pan, B.; Ding, B.; Fei, B.; Yi, X.; Chen, Y. A Meso-Mechanics-Based Experimental Method for Characterizing the in-Plane Compressive Properties of Aramid Paper. *Thin-Walled Struct.* **2021**, *162*, No. 107549.
- (49) Hao, B.; Zhang, Y.; Si, H.; Jiang, Z.; Li, C.; Zhang, Y.; Zhang, J.; Gong, C. Multiscale Design of Dielectric Composites for Enhanced Microwave Absorption Performance at Elevated Temperatures. *Adv. Funct. Mater.* **2025**, No. 2423897.
- (50) Hu, R.; He, X.; Luo, Y.; Liu, C.; Liu, S.; Lv, X.; Yan, J.; Peng, Y.; Yuan, M.; Che, R. Biomimetic Multi-Interface Design of Raspberry-Like Absorbent: Gd-Doped FeNi<sub>3</sub> @Covalent Organic Framework Derivatives for Efficient Electromagnetic Attenuation. *Small Methods* **2025**, *9*, No. 2401299.
- (51) Qin, M.; Zhang, L.; Wu, H. Dielectric Loss Mechanism in Electromagnetic Wave Absorbing Materials. *Adv. Sci.* **2022**, *9*, No. 2105553.
- (52) (a) Sun, H.; Yang, B.; Zhang, M. Functional–Structural Integrated Aramid Nanofiber-Based Honeycomb Materials with Ultrahigh Strength and Multi-Functionalities. *Adv. Fiber Mater.* **2024**, *6*, 1122–1137. (b) Feng, Z.; Liu, C.; Li, X.; Luo, G.; Zhai, N.; Hu, R.; Lin, J.; Peng, J.; Peng, Y.; Che, R. Designing Electronic Structures of Multiscale Helical Converters for Tailored Ultrabroad Electromagnetic Absorption. *Nano-Micro Lett.* **2025**, *17*, No. 20. (c) Lin, J.; Peng, Y.; Luo, J.; Xiong, Z.; Huang, J.; Zeng, X.; Wu, L.; Peng, J.; Liu, C. One-Click to 3D: Helical Carbon Nanotube-Mediated MXene Hierarchical Aerogel with Layer Spacing Engineering for Broadband Electromagnetic Wave Absorption. *Small Methods* **2024**, No. 2401665.
- (53) Feng, Z.; Liu, C.; Li, X.; Luo, G.; Zhai, N.; Hu, R.; Lin, J.; Peng, J.; Peng, Y.; Che, R. Designing Electronic Structures of Multiscale Helical Converters for Tailored Ultrabroad Electromagnetic Absorption. *Nano-Micro Lett.* **2025**, *17*, No. 20.
- (54) Lin, J.; Peng, Y.; Luo, J.; Xiong, Z.; Huang, J.; Zeng, X.; Wu, L.; Peng, J.; Liu, C. One-Click to 3D: Helical Carbon Nanotube-Mediated MXene Hierarchical Aerogel with Layer Spacing Engineering for Broadband Electromagnetic Wave Absorption. *Small Methods* **2024**, No. 2401665.